

Searching for dark matter axions via atomic excitations

J. D. Vergados

*University of Ioannina, Ioannina, Gr 451 10, Greece and Center for Axion
and Precision Physics Research, IBS, Daejeon 34051, Republic of Korea*

F.T. Avignone III and R. J. Creswick

University of South Carolina, Columbia, SC 29208, USA

S. Cohen

University of Ioannina, Ioannina, Gr 451 10, Greece

(Dated: December 8, 2022)

The possibility of axion detection by observing axion induced atomic excitations as suggested by Sikivie is discussed. The atom is cooled at low temperature and it is chosen to possess three levels. The first is the ground state, the second is completely empty chosen so that the energy difference between the two is close to the axion mass. Under the spin induced axion-electron interaction an electron is excited from the first to the second level. The presence of such an electron there can be confirmed by exciting it further via radiation of a suitably chosen photon energy to the appropriately selected third level, which is also empty, and lies at a higher excitation energy. From the observation of its subsequent de-excitation one infers the presence of the axion. The system is in a magnetic field so that the energies involved can be suitably adjusted. Since the axion is absorbed by the atom the cross section exhibits resonance behavior. Using an axion-electron coupling indicated by the limit obtained by the Borexino experiment, reasonable axion absorption rates have been obtained for various atomic targets.

PACS numbers: 93.35.+d 98.35.Gi 21.60.Cs

keywords:

Axion detection, axion dark matter, atomic excitations, B induced level splitting, ME of magnetic moment, narrow resonances, laser beams, frequency and magnetic field scan, event rate

I. INTRODUCTION

In the standard model there is a source of CP violation from the phase in the Kobayashi-Maskawa mixing matrix. This, however, is not large enough to explain the baryon asymmetry observed in nature. Another source is the phase in the interaction between gluons (θ -parameter), naively expected to be of order unity. The non observation of elementary electron dipole moment limits its value to be $\theta \leq 10^{-9}$. This has been known as the strong CP problem. A solution to this problem has been the P-Q (Peccei-Quinn) mechanism. In extensions of the S-M, e.g. two Higgs doublets, the Lagrangian has a global P-Q chiral symmetry $U_{PQ}(1)$, which is spontaneously broken, generating a Goldstone boson, the axion (a). In fact the axion has been proposed a long time ago as a solution to the strong CP problem [1] resulting to a pseudo Goldstone Boson [2, 3]. The two most widely cited models of invisible axions are the KSVZ (Kim, Shifman, Vainshtein and Zakharov) or hadronic axion models [4],[5] and the DFSZ (Dine, Fischler, Srednicki and Zhitnitskij) or GUT axion model [6],[7]. This also led to the interesting scenario of the axion being a candidate for dark matter in the universe [8–10] and it can be searched for by real experiments [11–14]. For a review see, see e.g., [15].

It has been recognized long time ago that the axion is an ideal cold dark matter candidate, especially in the mass range $10^{-6} \text{ eV} \leq m_a \leq 10^{-3} \text{ eV}$, by Sikivie [16], and others, see, e.g., [17]. Thus the popular experiments hope to detect them by their conversion to photons in the presence of a magnetic field (Primakoff effect), see Fig. 1(a),(b). The produced photons are detected in a resonance cavity as suggested by Sikivie [16]. In the case of the axion absorption by atoms, see Fig. 1(c), the detection can be achieved by directly measuring the photons following the atom de-excitation or as described in the text.

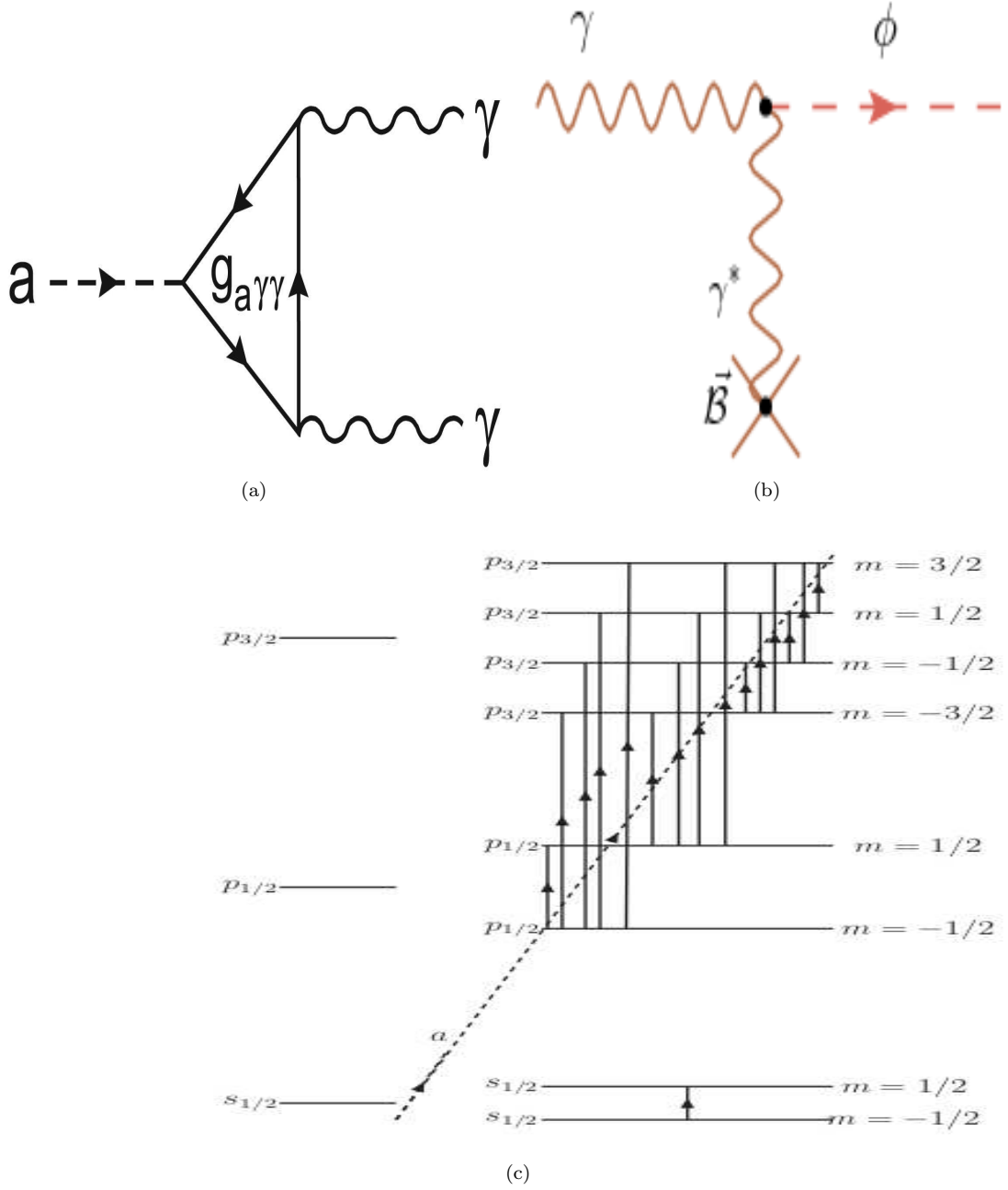


FIG. 1: (a) The axion to photon interaction, axion photon coupling. (b) The axion to photon conversion in the presence of a magnetic field, the Primakoff effect. (c) The axion absorption by an atom at low temperature, via the axion electron spin induced interaction. On the left the spectrum is as it appears in the absence of a magnetic field. On the right the energy splittings depend on the spin-orbit interaction and the magnitude of the magnetic field (the levels are not on scale). An electron is moved from an occupied initial level (anywhere the arrows begin) with energy E_i and angular momentum $n\ell j_i$ corresponding the substate $m_i = -j_i$ to a level with energy E_f with an angular momentum $n\ell j_f$, which may be anywhere the arrows provided that $m_f = -j_i + 0, \pm 1$ consistent with the angular momentum selection rules. The picture is drawn for one electron configurations, but it can be generalized to multi-electron configurations. In all cases only states with the same radial and orbital quantum numbers can be connected via the spin operator. When the total angular momentum of the two states is the same, the splitting is small and due to the magnetic field.

In fact various experiments¹ such as ADMX and ADMX-HF collaborations [11],[13],[20, 21] are planned and ongoing to search for them. In addition, the newly established center for axion and physics research (CAPP) has started an ambitious axion dark matter research program [22], using SQUID and HFET technologies [23]. Their strategy is to run several experiments in parallel to explore a wide range of axion masses with sensitivities better than the QCD axion models [24],[25],[26].

The allowed parameter space has been presented in a nice slide by Raffelt [27] in the Multidark-IBS workshop and, focusing on the axion as dark matter candidate, by Stern [20], derived from Fig. 3 of ref [20]).

Recently some exclusion on the axion masses have been obtained by the ADMX experiments in the range of 2.66-2.81 μeV [28], 2.81-3.39 μeV [29] and 3.3-4.2 μeV [30] leading to the exclusion of a wide range of axion-photon coupling values predicted in benchmark models of the invisible axion, which solve the strong CP problem of quantum chromodynamics.

Since, however, the mass of the axion is not known, it is important to consider other processes for its detection, which may be accessible to a wider window of axion mass. Such may involve, e.g., axion detection via atomic excitations [31], [32], [33].

In this paper we are going to discuss the possibility of axion detection by observing directly axion induced atomic excitations, measuring the photons produced in the de-excitation to the ground state, with sensitivity to axion masses in the range 10^{-5} eV close to 1 eV. Another procedure, suggested by Sikivie [34], involves an atom cooled at low temperature, which utilizes three energy levels. The first is the ground state. The second is completely empty, chosen such that the energy difference between the two is close to the axion mass. Under the spin induced axion-electron interaction an electron is excited from the first to the second level. The presence of such an electron there can be confirmed by exciting it further via radiation of suitably chosen photon energy to a third level, which is also empty, and lies at higher excitation energy. From the observation of its subsequent de-excitation one infers the presence of the axion (see Fig. 1c).

The magnetic field employed is used to split the magnetic m-substates so that the transition energies involved can be suitably adjusted. Furthermore, by suitably adjusting in size, it can determine a window of axion masses to be searched in given experiment

A crucial parameter in the axion induced atomic excitations is the axion electron coupling g_{ea}/f_a . The dimensionless quantity has been studied in axion models g_{ea} . The quantity f_a with dimension of mass is not known, but it is believed to be inversely proportional to the axion mass. In the present calculation we are going to adopt a value g_{ea}/f_a which coincides with the stringent limit obtained in the Borexino experiment [35]. We will see that this value leads to a very small cross section. Fortunately, we will find that experiments involving dark matter axions are not doomed to be un-observable, since the axion number density in our vicinity of the galaxy is quite large, owing to the small axion mass.

Our paper will be organized as follows: In section II we will derive expressions yielding the rates for axion absorption by atoms, in section III we will discuss the axion electron coupling and the range of the axion masses obtained from Borexino limit in conjunction with reasonable axion model parameters g_{ea} , in section IV we will study the obtained axion widths, in section V we will summarize the needed atomic physics input, in section VI we will consider the low temperature requirements for the success of the experiments, in section VII we will present our results for the expected rates and in section VIII we will summarize our conclusions.

II. EXPRESSIONS FOR RATES FOR AXION ABSORPTION BY ATOMS

We remind the reader that the axion, a , is a pseudoscalar particle and its coupling to the electron can be described by a Lagrangian of the form:

$$\mathcal{L} = \frac{g_e}{f_a} i \partial_\mu a \bar{\psi}(\mathbf{p}', s) \gamma^\mu \gamma_5 \psi(\mathbf{p}, s) \quad (1)$$

¹ Heavier axions with larger mass in the 1eV region produced thermally (such as via the $a\pi\pi\pi$ mechanism), e.g. in the sun, are also interesting and are searched by CERN Axion Solar Telescope (CAST) [18]. Other axion like particles (ALPs), with broken symmetries not connected to QCD, and dark photons form dark matter candidates called WISPs (Weakly Interacting Slim Particles) , see, e.g.,[19], are also being searched.

where g_e is a coupling constant and f_a a scale parameter with the dimension of energy. For an axion with mass m_a it easy to show that in the non relativistic limit:

- the time component $\mu = 0$ is given by:

$$\mathcal{L} = \langle \phi | \Omega | \phi \rangle, \Omega = \frac{g_e m_a}{2f_a} \frac{\boldsymbol{\sigma} \cdot \mathbf{q}}{m_e}, \mathbf{q} = \mathbf{p}' - \mathbf{p} \quad (2)$$

which is negligible for $m_a \ll m_e$.

- The space component, $\mu \neq 0$,

$$\mathcal{L}_{aee} = \langle \phi | \Omega | \phi \rangle, \Omega = \frac{g_e}{2f_a} \boldsymbol{\sigma} \cdot \mathbf{q}, \mathbf{q} = \mathbf{p}' - \mathbf{p} \quad (3)$$

where \mathbf{p} and \mathbf{p}' are the initial and final electron momenta, f_a the axion decay constant and $\boldsymbol{\sigma}$ the spin of the electron.

An interaction of the form of Eq. (2) has been proposed by Sikivie [34] as a way of detecting the axion by causing atomic excitations, g_{ae} is the relevant coupling constant to be determined by experiment.

The target is selected so that there exist two levels, say $|J_1, m_1\rangle$ and $|J_2, m_2\rangle$ which result from the splitting of the atomic levels by the magnetic field and they are characterized by the same n and ℓ so that they can be connected by the spin operator. The lower one $|J_1, m_1\rangle$ is occupied by electrons but the higher one $|J_2, m_2\rangle$ is completely empty at sufficiently low temperature. It can be populated only by exciting an electron to it from the lower one by the axion field. The occurrence of such an excitation is monitored by a tuned laser which excites such an electron from $|J_2, m_2\rangle$ to a higher state $|J_3, m_3\rangle$, which cannot be reached in any other way, by observing its subsequent decay.

In the present case we are interested in the case that the states $|J_1, m_1\rangle$ and $|J_2, m_2\rangle$ can be connected via the spin operator, i.e. the two states must have the same orbital structure and spins that can be reached by the spin operator (for single particle states, $J_1 = j_1$, $J_2 = j_2$, they must have the same n and ℓ quantum numbers). We distinguish to cases:

- $J_2 = J_1$. In this case the splitting is due to the magnetic field yielding about 10^{-4} eV/T. This is appropriate for detection of axions around this splitting for the chosen magnetic field.
- $J_2 \neq J_1$, i.e. they correspond to the two spin orbit partners. Then the energy splitting could be in the eV range and, thus, this arrangement is suitable for the detection of axions with mass in the same range.

Let us for simplicity assume a single particle transition. The relevant matrix element for the transition $j_1, m_1 \rightarrow j_2, m_2$ takes the form

$$\langle n\ell j_2 m_2 | \mathbf{q} \cdot \boldsymbol{\sigma} | n\ell j_1 m_1 \rangle = C_{\ell, j_1, m_1, J_2, m_2} q_{m_1 - m_2} I_{n\ell}(\mathbf{q}) \quad (4)$$

where $C_{\ell, j_1, m_1, j_2, m_2}$ depends on the atomic levels [36] and it will be given below, see section V, and $I_{n\ell}(\mathbf{q})$ is given by

$$I_{n\ell}(\mathbf{q}) = \int d^3\mathbf{p} \phi_{n\ell}(\mathbf{p} + \mathbf{q}) \phi_{n\ell}(\mathbf{p}) \quad (5)$$

Since the momentum transfer \mathbf{q} is small $I_{n\ell}(\mathbf{q}) \approx 1$. It can be shown that a similar result holds in the case of multi-particle configurations So the matrix element becomes

$$|\text{ME}(\mathbf{q})|^2 = \left(\frac{g_e}{2f_a} \right)^2 (C_{\ell, J_1, m_1, J_2, m_2})^2 \left(\delta_{m_1, m_2} q_0^2 + \frac{1}{2} (q_1^2 + q_2^2) (1 - \delta_{m_1, m_2}) \right) \quad (6)$$

where \mathbf{q} is the momentum transfer to the atom with q_0 its component in the direction of the axis of quantization and q_1, q_2 along the other two axes.

The cross section becomes

$$\sigma = \frac{1}{v} \frac{1}{2m_a} |\text{ME}(\mathbf{q})|^2 \int \int \frac{d^3\mathbf{p}_A}{(2\pi)^3} (2\pi)^3 \delta(\mathbf{q} - \mathbf{p}_A) 2\pi \delta(m_a + \frac{q^2}{2m_a} + E_i - E_f) \quad (7)$$

where \mathbf{p}_A the momentum transfer to the atom. $2m_a$ is the usual normalization for a boson field, In the above expression we have neglected the tiny recoiling energy of the atom. Thus

$$\sigma = \frac{1}{v} \frac{1}{2m_a} \left(\frac{g_e}{2f_a} \right)^2 (C_{\ell, j_1, m_1, j_2, m_2})^2 \left(\delta_{m_1, m_2} q_0^2 + \frac{1}{2} (q_1^2 + q_2^2) (1 - \delta_{m_1, m_2}) \right) 2\pi \delta(m_a + \frac{q^2}{2m_a} + E_i - E_f) \quad (8)$$

We will now fold the cross section with the axion velocity distribution, assuming that with respect to the galactic center is of the Maxwell-Boltzmann type:

$$f_g(v') = \frac{1}{v_0^3} \frac{1}{\pi \sqrt{\pi}} e^{-\left(\frac{v'}{v_0}\right)^2} \quad (9)$$

In the local frame, ignoring for the moment the motion of the Earth, we have $\mathbf{v}' \rightarrow \mathbf{v} + v_0 \hat{z}$

$$f_\ell(\mathbf{v}) = \frac{1}{v_0^3} \frac{1}{\pi \sqrt{\pi}} e^{-(y^2 + 2y\xi + 1)}, \quad y = \frac{v}{v_0} \quad (10)$$

The integration over the velocity distribution we find:

$$\langle y\sigma \rangle = \frac{1}{2m_a} \left(\frac{g_e}{2f_a} \right)^2 (C_{\ell, j_1, m_1, j_2, m_2}) \Lambda \quad (11)$$

where

$$\begin{aligned} \Lambda &= \frac{1}{v_0} \int y f(\mathbf{v}) d^3\mathbf{v} \left(\delta_{m_1, m_2} q_0^2 + \frac{1}{2} (q_1^2 + q_2^2) (1 - \delta_{m_1, m_2}) \right) 2\pi \delta(m_a (1 + \frac{1}{2} v^2) + E_i - E_f) \\ &= \int y dy y^2 (m_a v_0 y)^2 2\pi \delta(m_a (1 + \frac{1}{2} v_0^2 y^2) + E_i - E_f) J \frac{1}{(\sqrt{\pi})^3}, \\ J_1 &= \int d\Omega e^{-(y^2 + 2y\xi + 1)} \left(\delta_{m_1, m_2} \xi^2 + \frac{1}{2} (1 - \xi^2) (1 - \delta_{m_1, m_2}) \right) \end{aligned} \quad (12)$$

So the integration over the angles yields:

- In the galactic frame

$$J_1 = 2\pi J, \quad J = e^{-y^2} 2\pi \int d\xi \left(\delta_{m_1, m_2} \xi^2 + \frac{1}{2} (1 - \xi^2) (1 - \delta_{m_1, m_2}) \right) = \frac{4\pi}{3} e^{-y^2} \quad (13)$$

which is symmetric.

- in the local frame we get:

$$J_1 = 2\pi J, \quad J = e^{-1-y^2} 2\pi \int d\xi e^{-2y\xi} \left(\delta_{m_1, m_2} \xi^2 + \frac{1}{2} (1 - \xi^2) (1 - \delta_{m_1, m_2}) \right) \quad (14)$$

that is

$$J = e^{-1-y^2} \left(\delta_{m_1, m_2} \frac{(2y^2 + 1) \sinh(2y) - 2y \cosh(2y)}{2y^3} + (1 - \delta_{m_1, m_2}) \frac{2y \cosh(2y) - \sinh(2y)}{4y^3} \right) \quad (15)$$

The integration over the magnitude of the velocity is trivial due to the δ function appearing in Eq. (12). We thus get in the local frame:

$$\Lambda = 4\sqrt{\pi} m_a \frac{1}{v_0} F_{m_1, m_2}(X), \quad F_{m_1, m_2}(X) = \begin{cases} \frac{1}{2} X e^{-X^2-1} ((2X^2 + 1) \sinh(2X) - 2X \cosh(2X)), & m_1 = m_2 \\ \frac{1}{4} X e^{-X^2-1} (2X \cosh(2X) - \sinh(2X)), & m_1 \neq m_2 \end{cases} \quad (16)$$

The extra factor of X^4 in going from Eq. (15) to Eq. (16) is the result of the integration over the velocity.

Sometimes we prefer to normalize the function $F_{m_1, m_2}(X)$. Then we write

$$\Lambda = 4\sqrt{\pi} m_a \frac{1}{v_0} N_{m_1, m_2} F_{m_1, m_2}^N(X), \quad N_{m_1, m_2} = \begin{cases} \frac{1}{2} \sqrt{\pi} \text{erf}(1), & m_1 = m_2 \\ \frac{e\sqrt{\pi} \text{erf}(1)+2}{8e}, & m_1 \neq m_2 \end{cases} \quad (17)$$

In Eq. (17) $F_{m_1, m_2}^N(X)$ is a function of X given by

$$F_{m_1, m_2}^N(X) = \begin{cases} \frac{X e^{-X^2-1} ((2X^2+1) \sinh(2X) - 2X \cosh(2X))}{\sqrt{\pi} \operatorname{erf}(1)}, & m_1 = m_2 \\ \frac{2X e^{-X^2} (2X \cosh(2X) - \sinh(2X))}{e \sqrt{\pi} \operatorname{erf}(1) + 2}, & m_1 \neq m_2 \end{cases} \quad (18)$$

with X given by:

$$X = \frac{c}{v_0} \left(\sqrt{2 \left(\frac{E_f - E_i}{m_a c^2} - 1 \right)} \right). \quad (19)$$

Thus one obtains:

$$\langle y\sigma \rangle = \frac{1}{2} \frac{1}{v_0} \left(\frac{g_e}{f_a} \right)^2 4\sqrt{\pi} (C_{\ell, j_1, m_1, j_2, m_2})^2 F_{m_1, m_2}(X). \quad (20)$$

The event associated with a flux of particles with velocity v (per atom in the target) is given by:

$$R = \Phi_a \sigma \quad (21)$$

where Φ_a is the axion flux given by $\Phi_a = \frac{\rho_a}{m_a} v_0$ with ρ_a the axion matter density in our vicinity of the galaxy. In this work we will assume that all dark matter in our vicinity is composed of axions. So it is obtained from the rotation curves and employed in standard dark matter searches, i.e. $\rho_a = 0.3 \text{ GeV/cm}^3$. This leads to a large axion particle density $\frac{\rho_a}{m_a}$ due to the smallness of the axion mass.

Thus averaging over the velocity distribution we get per atom

$$\langle R \rangle = \frac{\rho_a}{m_a} v_0 \langle y\sigma \rangle \quad (22)$$

Thus Eq. (21) for N atoms in the target becomes

$$R = R_0(m_a) (C_{\ell, j_1, m_1, j_2, m_2})^2 F_{m_1, m_2}(X), R_0(m_a) = \Phi_0(m_a) \sigma_0, \Phi_0(m_a) = N \frac{\rho_a}{m_a} v_0, \sigma_0 = 2\sqrt{\pi} \frac{1}{v_0} \frac{g_{ae}^2}{f_a^2} \quad (23)$$

$R_0(m_a)$ is written as a product of two constants, one with the dimension of the flux, which varies inversely proportional to the axion mass and the other yields the scale of the cross section.

III. THE AXION ELECTRON COUPLING

A crucial parameter in the present work is $\frac{g_{ae}}{f_a}$. In the past this parameter was derived from existing axion models. In a recent paper [35] the following limits were obtained:

$$|g_{Ae} \times m_A| \leq 2.0 \times 10^{-5} \text{ eV}, |g_{Ae} \times g_{3AN}| \leq 5.5 \times 10^{-13} \text{ eV}. \quad (24)$$

These can be interpreted to be the axion electron and the isovector axion nucleon coupling, which in our notation are written:

$$|g_{ae} \times m_a| \leq 2.0 \times 10^{-5} \text{ eV}, |g_{aN}^3| \leq 2.8 \times 10^{-8} \text{ eV} \quad (25)$$

Using now the equation [37], [38]

$$m_a f_a \approx 6000 \text{ MeV}^2 \quad (26)$$

we obtain

$$\frac{g_{ae}}{f_a} \leq 3.3 \times 10^{-12} \text{ GeV}^{-1}, \frac{g_{aN}^3}{f_a} \leq 4.7 \times 10^{-15} \text{ GeV}^{-1} \quad (27)$$

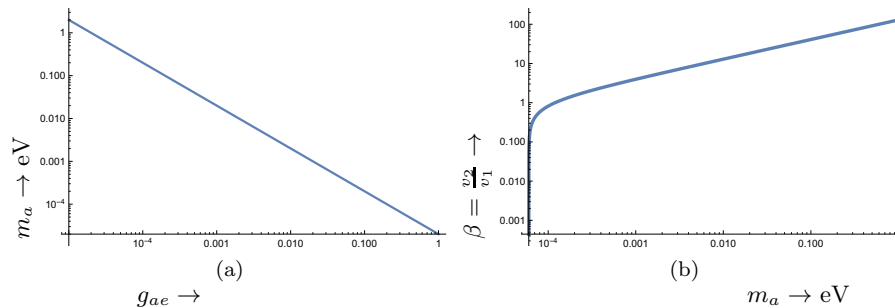


FIG. 2: (a) The axion mass m_a allowed by the coupling given in Eq. (25) as a function of g_{ae} . This covers the whole range of m_a of interest in this work. (b) The ratio $\beta = \frac{v_2}{v_1}$ of the expectation values of the Higgs doublets of the DFSZ axion model discussed in the text. as a function of the axion mass m_a .

These couplings are indeed very small. This perhaps explains why for the Borexino 5.5 MeV solar axion flux on Earth, resulting from the second relation of the equation, is very small. This is the reason why, in our recently published paper [38] we had to admit that the nuclear excitations were not detectable. This, of course did not affect the atomic excitations discussed in the same paper, since the axion flux for the 14.4 keV solar axions, used in this paper, happened to be much larger. Anyway in the present calculation we consider dark matter axions with flux of a different origin.

The coupling g_{ae} is not known. but it has been investigated [39, 40], in particular in the context of the DFSZ axion models [7, 9]. This leads to:

$$g_e = \frac{1}{3} \left(1 - \frac{\tan^2 \beta}{1 + \tan^2 \beta} \right), \tan \beta = \frac{v_2}{v_1} \text{ or } g_e = \frac{1}{3} \cos^2 \beta \quad (28)$$

Where $\tan \beta$ is the ratio of the vacuum expectation values of the two doublets of the model, the parameter β is not known, but some sort of theoretical limits exist [41], e.g. $\frac{1}{6} < g_e < \frac{1}{3}$.

In the present work we will assume that the upper limit of Eq. (25) corresponds to the actual value of $g_{ae} m_a$. Then, since the overall coupling in Eq. (25) depends on both the axion mass and the coupling g_{ae} , we obtain a range for the axion mass, see Fig. 2(a). Having such a range of axion mass, it is amusing to note that once the axion mass is determined one can determine the ratio $\beta = \frac{v_2}{v_1}$, see Fig. 2(b).

Anyway from Eq. (25), using e.g. $g_{ae} = \frac{1}{6}$, one finds $f_a = 5 \times 10^{10}$ GeV. Using this information one finds the scale of the cross to be $\sigma_0 = 2 \times 10^{-47} \text{ cm}^2$. Furthermore for $N = 6.0 \times 10^{23}$ atoms in one mol and the axion flux in our vicinity being $\Phi_0 = \tilde{\Phi}_0/m_a$ with $\tilde{\Phi}_0 = 2.0 \times 10^{23} \frac{1 \text{ eV}}{\text{y (cm)}^2}$, one finds one finds $R_0(m_a) = (N\Phi_0\sigma_0) = 2.55 \frac{1 \text{ eV}}{m_a}$ per mol-y. Thus the main axion mass dependence of the event is as shown in Fig. 3.

Additional axion mass dependence, which can be exploited by experiment, is contained in $F_{m_1, m_2}(X)$ through X , see Eq. (19).

IV. THE AXION ABSORPTION WIDTHS

Since the axion is absorbed one expects the cross section to exhibit a resonance behavior. This is exhibited by considering the function $F_{m_1, m_2}^N(X)$ in the variable X , which depends on the energy difference of the atomic levels, the axion mass and the velocity of the sun around the center of the galaxy. The energy difference depends, of course, on the magnetic quantum numbers m_1 and m_2 of the states involved.

The overall behavior of the functions $F_{m_1, m_2}^N(X)$ is exhibited in Fig. 4. In fact we find that the characteristics of the resonance are:

$$\begin{cases} \Gamma = 1.35, & \langle X \rangle = 1.9, & \text{local frame, } m_1 = m_2 \\ \Gamma = 1.35, & \langle X \rangle = 1.7, & \text{local frame, } m_1 \neq m_2 \end{cases}, \quad (29)$$

where $\langle X \rangle$ is the location of the maximum

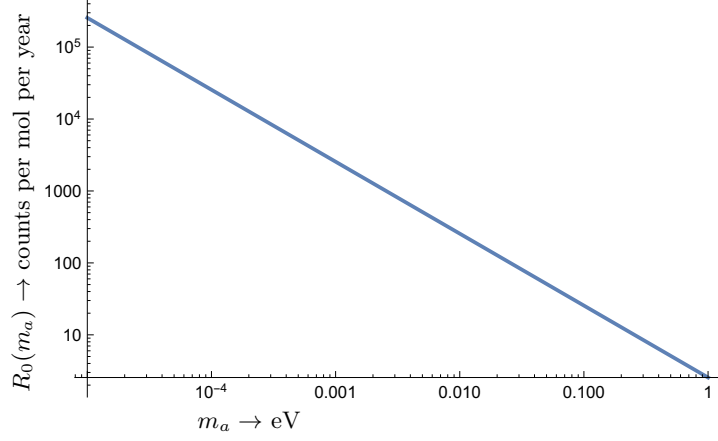


FIG. 3: The scale of the rate as a function of the axion mass.

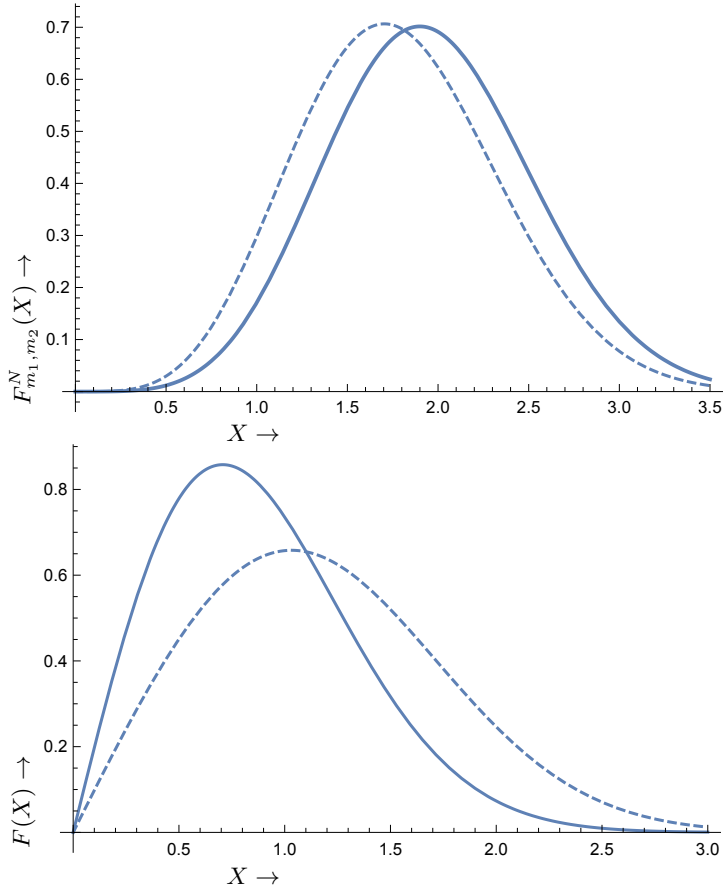


FIG. 4: Top panel: The normalized distribution $F_{m_1, m_2}^N(X)$ as a function of X , $X = \frac{c}{v_0} \left(\sqrt{2 \left(\frac{E_f - E_i}{m_a c^2} - 1 \right)} \right)$ with v_0 the velocity of the sun around the center of the galaxy in natural units, 0.7×10^{-3} . The solid line holds for $m_1 = m_2$, while the dashed line for $m_2 = m_1 \pm 1$. The widths are the same $\Gamma = 1.35$ for both cases. The corresponding values of $\langle X \rangle$ are 1.9 and 1.7 for the solid and dashed curve respectively. Bottom panel: For comparison the normalized distribution $F(X)$ $X = \frac{c}{v_0} \left(\sqrt{2 \left(\frac{\omega}{m_a c^2} - 1 \right)} \right)$, with ω the photon energy, in the case of the standard axion to photon conversion is presented, obtained with the same halo parameters as in the top panel, in the galactic frame (solid curve) and local frame. (dashed curve)

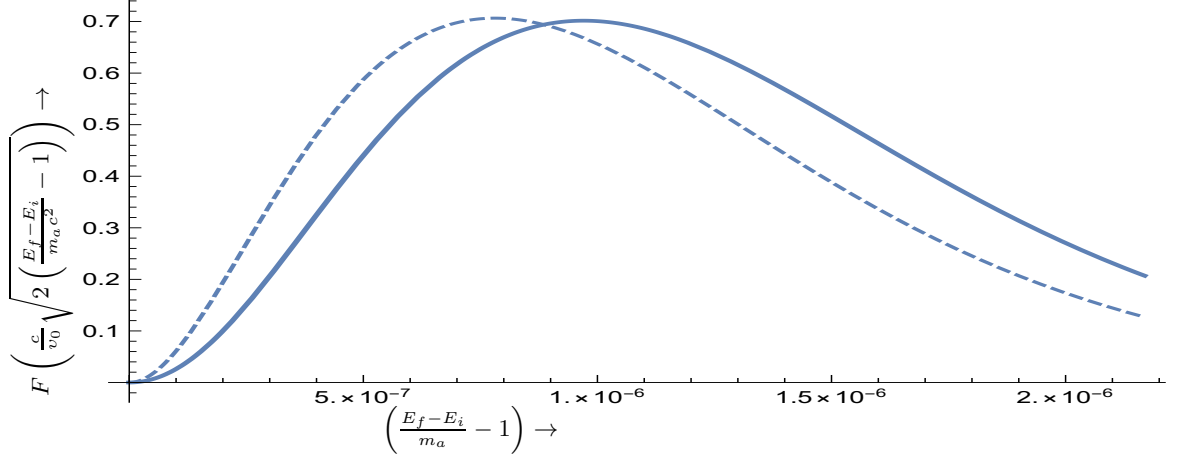


FIG. 5: The cross section exhibits resonance behavior. Shown is $F(X)$ as a function of $\left(\frac{E_f - E_i}{m_a c^2} - 1\right)$. The solid line corresponds to $m_1 = m_2$, while the dashed line corresponds to $m_1 \neq m_2$, both in the local frame.

We have seen that we have resonance behavior in the variable X . At the location of the maximum from the relation $\langle X \rangle = \frac{c}{v_0} \left(\sqrt{2 \left(\frac{E_f - E_i}{m_a c^2} - 1 \right)} \right)$ we find that

$$m_a = (E_f - E_i)(1 - \chi), \chi = 0.27 \times 10^{-6} \langle X \rangle^2 \text{ i.e. } \begin{cases} \chi = 0.97 \times 10^{-6}, & m_1 = m_2 \\ \chi = 0.78 \times 10^{-6}, & m_1 \neq m_2 \end{cases} \quad (30)$$

For all practical purposes the axion mass is equal to the excitation energy. Furthermore

$$\frac{E_f - E_i}{m_a} = (1 + \chi), \chi = 0.27 \times 10^{-6} \langle X \rangle^2 \text{ i.e. } \begin{cases} \chi = 0.97 \times 10^{-6}, & m_1 = m_2 \\ \chi = 0.88 \times 10^{-6}, & m_1 \neq m_2 \end{cases} \quad (31)$$

Similarly we can find the width in the energy space for both types of transitions. Thus

$$X_1 = 1.067 \leftrightarrow \left(\frac{E_f - E_i}{m_a} \right)_1 = (1 + 0.306 \times 10^{-6}), X_2 = 2.417 \leftrightarrow \left(\frac{E_f - E_i}{m_a} \right)_2 = (1 + 1.566 \times 10^{-6}) \Rightarrow$$

$$\Gamma_E = \left(\frac{E_f - E_i}{m_a} \right)_2 - \left(\frac{E_f - E_i}{m_a} \right)_1 = ((1 + 1.566 \times 10^{-6}) - (1 + 0.306 \times 10^{-6})) = 1.26 \times 10^{-6} \quad (32)$$

At $X = 0$ we find that at $\frac{E_f - E_i}{m_a} = 1$ the distribution vanishes. On the other hand at $X = 2.84$ i.e. for $\frac{E_f - E_i}{m_a} = 1 + 2 \times 10^{-6}$, the distribution almost vanishes². In other words the distribution vanishes at $X = 0$ and at $X = 2.84$ after having gone very rapidly through $\langle X \rangle$ with a width as given by Eq. (32). Anyway the above picture emerges more clearly by plotting the function $F(X)$ as a function of the energy $(E_f - E_i)/m_a c^2$, see Fig. 5.

We have seen that the axion mass is very close to the excitation energy. Since the resonance is so narrow, however, special care is required not to miss it. Some experimental arrangement to facilitate the observation of such a narrow resonance from the expected atomic spectra will be considered below, see section VII. Furthermore on this end the experience gained with the axion to photon conversion experiments involving resonance cavities, such as ADMX and ADMX-HF collaborations [11],[13],[20, 21] and CAPP [22], [23], [24],[25],[26], may be very helpful. The observation of the resonance is very important, among other things, to discriminate against background. It is very unlikely that background events will simulate a similar resonance pattern with that that obtained here, reflecting not only the

² There is no need to go to values of $X > y_{esc} = 2.84$, since velocities above the escape velocity, $v > v_{esc} = y_{esc} v_0$, in the Maxwell-Boltzmann distribution have been excluded.

Maxwell-Boltzmann distribution, but the momentum dependence of the axion electron system as well. Furthermore, given enough counts, one can exploit, if it becomes necessary, the extra signature, provided by the fact that the resonance width exhibits time dependence, i.e. an annual modulation due to the motion of Earth, see [42] and the Appendix, section IX.

Before completing this section we should mention that resonance plots, correlated with the event rate, will be specialized in section VII for the various atomic targets considered in this work.

V. ATOMIC PHYSICS CONSIDERATIONS

We will consider some atomic targets which possess two features. The ground state is composed of a multiplet of the form $n^{2S+1}L_{J_1}, S \neq 0$ while the excited state is of the form $n^{2S+1}L_{J_2}$ with $|J_1 - 1| \leq J_2 \leq J_1 + 1$, so that it can be reached by spin excitations.

The following types of excitations are in principle possible:

- $|J_1, -J_1\rangle \rightarrow |J_1, -J_1 + 1\rangle$, indicated as type A
- $|J_1, -J_1\rangle \rightarrow |J_2, -J_1 - 1\rangle$, indicated as type B
- $|J_1, -J_1\rangle \rightarrow |J_2, -J_1\rangle$, indicated as type C
- $|J_1, -J_1\rangle \rightarrow |J_2, -J_1 + 1\rangle$, indicated as type D

As we will see below some of these types may not be allowed by the angular momentum selection rules. Thus, e.g., for states $s_{1/2}$ single particle states only the A type is possible. For many electron configurations see subsection V B.

A. Single particle spin orbit partners

The ground state is a single particle state is of the form $n\ell j_1, j_1 = |\ell - 1/2|$ while the state $n\ell j_2, j_2 = \ell + 1/2$ is empty. Such examples can be found in the atomic data.

Since this is an one body transition, $J_1 = j_1, J_2 = j_2$ the relevant matrix element takes the form:

$$C_{\ell, j_1, m_1, j_2, m_2} = \langle j_1 m_1, 1 m_2 - m_1 | j_2 m_2 \rangle \sqrt{(2j_1 + 1)3} \sqrt{2\ell + 1} \sqrt{6} \begin{Bmatrix} \ell & \frac{1}{2} & j_1 \\ \ell & \frac{1}{2} & j_2 \\ 0 & 1 & 1 \end{Bmatrix} (-1)^{m_1 - m_2} \quad (33)$$

i.e. it simply expressed in terms of a Glebsch-Gordan coefficient and the nine- j symbol. We are interested in the case $j_1, m_1 = j_1, -J_1$. The relevant coefficients are tabulated in table I.

i) First we will consider a target with the ground state being a single $p_{1/2}$ orbital, while the $p_{3/2}$ is empty. Let us suppose that the spin orbit splitting is ϵ_p . In the presence of a magnetic field the m-degeneracy is removed and the ground state is in the state $|j_1, m_1\rangle = |1/2, -1/2\rangle$. Then we have the following spin induced transitions:

$$|1/2, -1/2\rangle \rightarrow |1/2, 1/2\rangle, |1/2, -1/2\rangle \rightarrow |3/2, -3/2\rangle, |1/2, -1/2\rangle \rightarrow |3/2, -1/2\rangle, |1/2, -1/2\rangle \rightarrow |3/2, 1/2\rangle$$

indicated as as above, i.e. A,B,C and D respectively. Thus the transition energies are

$$m = \left\{ 2\delta, \epsilon - \delta, \frac{\delta}{3} + \epsilon, \frac{5\delta}{3} + \epsilon \right\}, \epsilon = \epsilon_p \quad (34)$$

where we have included both the spin and orbital magnetic moments with $\delta = B\mu_B$ with μ_B the Bohr magneton and B the magnetic field. For a field of 1T we find $\delta = 5.788 \times 10^{-5}$ eV, i.e.

$$\delta = 5.788 \times 10^{-5} \frac{B}{1\text{T}} \text{eV} \quad (35)$$

A good candidate for such a transition is $_{13}\text{Al}$, involving the orbitals $3p_{1/2}$ and $3p_{3/2}$. From existing tables

(<https://www.nist.gov/pml/atomic-spectra-database>) we find $\epsilon_p = 0.0139$ eV. The spin induced matrix elements are as follows

$$C = \{2/9, 4/3, 8/9, 4/9\} \text{ for the } A, B, C, D \text{ respectively}$$

ii) Next we will consider a target with the ground state containing a single $d_{3/2}$ orbital, while the $d_{5/2}$ is empty. Let us suppose that the spin orbit splitting is ϵ_d . In the presence of a magnetic field the m-degeneracy is removed and the ground state is in the state $|j_1, m_1\rangle = |3/2, -3/2\rangle$. Then we have the following spin induced transitions:

$$|3/2, -3/2\rangle \rightarrow |3/2, 1/2\rangle, |3/2, -3/2\rangle \rightarrow |5/2, -5/2\rangle, |3/2, -3/2\rangle \rightarrow |5/2, -3/2\rangle, |3/2, -3/2\rangle \rightarrow |5/2, -1/2\rangle$$

indicated again as A,B,C and D respectively. Thus the excitation energies are:

$$m = \left\{ \frac{8\delta}{5}, \epsilon - \frac{2\delta}{5}, \frac{6\delta}{5} + \epsilon, \frac{16\delta}{5} + \epsilon \right\}, \epsilon = \epsilon_d \quad (36)$$

where we have included both spin and orbital magnetic moment

Our best candidate found in the above reference is the target ^{21}Sc involving the $3d_{3/2} \rightarrow 3d_{5/2}$ transitions with $\epsilon_d = 0.021$ eV. Other candidates can also be found in the same reference, e.g.: Z=39 (Y I, $4d_{3/2}d_{5/2}$, 0.066 eV) and Z=71 (Lu I, $5d_{3/2}d_{5/2}$, 0.25 eV) where I indicates that it is a neutral atom.

We thus we can use Eq. (36) with the appropriate value of ϵ_d and the spin induced $|\text{ME}|^2$

$$C = \{4/25, 8/5, 16/25, 4/25\}$$

iii) $s_{1/2}$ states. Such states exist in many atomic targets. In all such cases

$$m = 2\delta, C = 2.$$

We note the relatively large spin matrix for single particle excitations.

Note that in the case of $s_{1/2}$ and the A type transitions the lowest value of the WIMP mass required for the process to take place is very small, since the spin orbit splitting does not appear. If such configuration exists in the ground state of the atom considered, the obtained results are independent of the atom.

The transition energy is also small for the other type of transitions, if the spin orbit splitting is small as, e.g., in the case for all 3d-transitions considered here.

B. More than one electron configurations

1. Two electron configurations

The simplest possible case is two electron configurations. Now the needed states are spin symmetric. Antisymmetry of the wave functions requires the space part to be antisymmetric, i.e. a wave function of the form

$$\psi = \phi_{n\ell}^2(r) [L = \text{odd}, S = 1] J = L - 1, L, L + 1$$

i.e. spin triplet and L odd states.

Of special interest are the cases involving the functions:

$$\psi = \phi_{n\ell}^2(r)^3 P_J, \quad \phi_{n\ell}^2(r)^3 F_J$$

Then the spin matrix element can be cast in form:

$$C_{L, J_1, m_1, J_2, m_2} = \langle {}^3L_{J_2 m_2} | \sigma | {}^3L_{J_1 m_1} \rangle = \frac{1}{\sqrt{2J_2 + 1}} \langle J_1 m_1, 1 m_2 - m_1 | J_2 m_2 \rangle \langle {}^3L_{J_2} | |\sigma| | {}^3L_{J_1} \rangle, L = P, F \quad (37)$$

Good candidates are the following:

i) $L = 1$.

In this case the gs of the carbon atom is of the form $2s^2 2p^2 {}^3P_0$, while the excited state which can be populated by

spin excitations is 3P_1 at 16.41671 cm^{-1} , about 0.002 eV . It may be useful to note that the silicon atom (Si I) has the same structure, except for the radial quantum number $n = 3$ and the fact that $\epsilon = 0.00956 \text{ eV}$. The first does not affect the calculations performed here, while the second can be selected on the basis of the axion mass is being searched. That being said, the experimenters can choose whichever is more appropriate for them.

So since in both cases the initial state is not degenerate, the only excitations are $0 \rightarrow m$ caused by the spin σ_m appear. Furthermore one need consider of the splitting of the final multiplet $2s^22p^2{}^3P_1$, which is given by

$$\left\{ -\frac{3\delta}{2}, 0, \frac{3\delta}{2} \right\} \text{ for } m = -1, 0, 1 \text{ respectively.}$$

Thus in the case of carbon

$$m = \left\{ -\frac{3\delta}{2} + \epsilon, 0, \frac{3\delta}{2} + \epsilon \right\}, \epsilon = 0.002 \text{ eV} \quad (38)$$

ii) $L = 3$

A good such candidate is the Ti atom. In this case the gs is of the form $4s^23d^2{}^3F_2$. The excited state that can be reached is 3F_3 at $170.134 \text{ cm}^{-1} = 0.02 \text{ eV}$. Another good candidate is the neutral Zirconium (Zr I) atom. This has the same structure, except for the radial quantum being $n = 5$, which is irrelevant for our calculations, and the fact that $\epsilon = 0.0707 \text{ eV}$. The latter affects the axion mass to be extracted by the experimenters. So the choice of the target can be selected on the basis of the same criteria as above. Thus for both cases

$$m = \left\{ \frac{28\delta}{9}, \frac{121\delta}{72} + \epsilon, \frac{115\delta}{36} + \epsilon, \frac{113\delta}{24} + \epsilon \right\}, \quad (39)$$

including both the spin and the orbital magnetic moment with ϵ the two values just mentioned.

The relevant spin matrix element is given in table II.

2. More than two electron configurations

i) The oxygen atom.

In this case the gs is of the form $2s^22p^4{}^3P_2$, while the excited state which can be populated by spin excitations is 3P_1 at 158.265 cm^{-1} , about 0.0196 eV . This target is appropriate at the low temperatures we consider, since it is no longer a gas. Otherwise one might consider the atom of Sulfur (S I) which has the same configuration but with $n=3$ instead of $n=2$. Returning to the oxygen atom, we will consider of the splitting of the ground state multiplet $2s^22p^4{}^3P_2$, as well as the final state multiplet $2s^22p^4{}^3P_1$

By angular momentum selection rules only the A and the D terms are allowed. Thus one finds

$$m = \left\{ \frac{5\delta}{3}, 0, 0, \frac{5\delta}{3} + \epsilon \right\}, \epsilon = 0.0196 \text{ eV.} \quad (40)$$

including the contribution of both the spin and orbital magnetic moment.

ii) The ${}_{26}\text{Fe}$ atom.

$3d^64s^2{}^5D_4$ while the excited state that can be populated by spin excitations is the first excited state 5D_3 at $415.933 \text{ cm}^{-1} = 0.05 \text{ eV}$. The calculation of the reduced spin and orbital angular momentum matrix elements is a bit complicated, but it can be simplified by making use of the symmetries of the wave functions. The spin part is characterized by the $\text{SU}(2)$ symmetry [5, 1] while antisymmetry requires the orbital part to be $[2, 1^4]$ under $\text{SU}(5)$. The relevant matrix elements can be evaluated using standard techniques, see e.g [43], making use of table B.19. Since only the transitions of the type A and D appear in this case, one finds

$$m = \left\{ \frac{16\delta}{5}, 0, 0, \frac{16\delta}{5} + \epsilon \right\}, \epsilon = 0.05 \text{ eV} \quad (41)$$

including both the spin and the orbital magnetic moments.

The needed spin induced transition matrix elements $\langle {}^3P_{J_2m_2} | \sigma | {}^3P_{J_1, -J_1} \rangle^2$ and $\langle {}^3F_{J_2m_2} | \sigma | {}^3F_{J_1, -J_1} \rangle^2$ and $\langle {}^5D_{J_2m_2} | \sigma | {}^5D_{J_1, -J_1} \rangle^2$ are shown in II

TABLE I: The coefficients $(C_{j_1, m_1, j_2, m_2, \ell})^2$ connecting via the spin operator a given initial state $|i\rangle = |n\ell, j_1, -j_1\rangle$ with all possible states $|f\rangle = |n\ell, j_2, m_2\rangle$, for $\ell = 0, 1, 2, 3$.

$ i\rangle$		$ f\rangle$		$C_{j_1, m_1, j_2, m_2, \ell}^2$	
ℓ	j_1	m_1	j_2		m_2
0	$\frac{1}{2}$	$-\frac{1}{2}$	$\frac{1}{2}$	$\frac{1}{2}$	2
1	$\frac{1}{2}$	$-\frac{1}{2}$	$\frac{1}{2}$	$\frac{1}{2}$	$\frac{2}{9}$
1	$\frac{1}{2}$	$-\frac{1}{2}$	$\frac{3}{2}$	$\frac{3}{2}$	$\frac{4}{9}$
1	$\frac{1}{2}$	$-\frac{1}{2}$	$\frac{3}{2}$	$-\frac{3}{2}$	$\frac{4}{9}$
1	$\frac{1}{2}$	$-\frac{1}{2}$	$\frac{3}{2}$	$-\frac{1}{2}$	$\frac{2}{3}$
1	$\frac{1}{2}$	$-\frac{1}{2}$	$\frac{3}{2}$	$\frac{1}{2}$	$\frac{2}{3}$
2	$\frac{3}{2}$	$-\frac{3}{2}$	$\frac{3}{2}$	$\frac{1}{2}$	$\frac{8}{25}$
2	$\frac{3}{2}$	$-\frac{3}{2}$	$\frac{3}{2}$	$-\frac{1}{2}$	$\frac{8}{25}$
2	$\frac{3}{2}$	$-\frac{3}{2}$	$\frac{5}{2}$	$\frac{5}{2}$	$\frac{16}{25}$
2	$\frac{3}{2}$	$-\frac{3}{2}$	$\frac{5}{2}$	$-\frac{5}{2}$	$\frac{16}{25}$
2	$\frac{3}{2}$	$-\frac{3}{2}$	$\frac{5}{2}$	$-\frac{3}{2}$	$\frac{10}{25}$
2	$\frac{3}{2}$	$-\frac{3}{2}$	$\frac{5}{2}$	$\frac{3}{2}$	$\frac{10}{25}$
3	$\frac{5}{2}$	$-\frac{5}{2}$	$\frac{5}{2}$	$-\frac{3}{2}$	$\frac{49}{10}$
3	$\frac{5}{2}$	$-\frac{5}{2}$	$\frac{5}{2}$	$-\frac{1}{2}$	$\frac{49}{10}$
3	$\frac{5}{2}$	$-\frac{5}{2}$	$\frac{7}{2}$	$\frac{7}{2}$	$\frac{24}{49}$
3	$\frac{5}{2}$	$-\frac{5}{2}$	$\frac{7}{2}$	$-\frac{7}{2}$	$\frac{24}{49}$
3	$\frac{5}{2}$	$-\frac{5}{2}$	$\frac{7}{2}$	$-\frac{5}{2}$	$\frac{49}{49}$

TABLE II: The coefficients $\langle {}^3P_{J_2} || \sigma || {}^3P_{J_1} \rangle$, $\langle {}^3F_{J_2} || \sigma || {}^3F_{J_1} \rangle$ and $\langle {}^5D_{J_2} || \sigma || {}^5D_{J_1} \rangle$ as well as the corresponding total matrix elements $|ME|^2$ relevant to the present work. Note that the initial sub-state is of the form $|j_1, m_1\rangle = |J_1, -J_1\rangle$

J_1	J_2	$\langle {}^3P_{J_2} \sigma {}^3P_{J_1} \rangle$	m_1	q	$\frac{\langle J_1, m_1 1, 1q J_2, m_1 + q \rangle}{\sqrt{2J_2 + 1}}$	$ ME ^2$
0	1	$2\sqrt{2}$	0	$\pm 1, 0$	$\frac{1}{\sqrt{3}}$	8/3

J_1	J_2	$\langle {}^3F_{J_2} \sigma {}^3F_{J_1} \rangle$	m_1	q	$\frac{\langle J_1, m_1 1, 1q J_2, m_1 + q \rangle}{\sqrt{2J_2 + 1}}$	$ ME ^2$
2	2	$-2\sqrt{\frac{10}{3}}$	-2	1	$-\frac{1}{\sqrt{15}}$	$\frac{8}{9}$
2	3	$-4\sqrt{\frac{5}{3}}$	-2	-1	$\frac{1}{\sqrt{7}}$	$\frac{80}{21}$
2	3	$-4\sqrt{\frac{5}{3}}$	-2	0	$\frac{1}{\sqrt{21}}$	$\frac{80}{63}$
2	3	$-4\sqrt{\frac{5}{3}}$	-2	1	$\frac{1}{\sqrt{105}}$	$\frac{16}{63}$

J_1	J_2	$\langle {}^3P_{J_2} \sigma {}^3P_{J_1} \rangle$	m_1	q	$\frac{\langle J_1, m_1 1, 1q J_2, m_1 + q \rangle}{\sqrt{2J_2 + 1}}$	$ ME ^2$
2	2	$\sqrt{30}$	-2	1	$-\frac{1}{\sqrt{15}}$	2
2	1	$\sqrt{10}$	-2	1	$\frac{1}{\sqrt{5}}$	2

J_1	J_2	$\langle {}^5D_{J_2} \sigma {}^5D_{J_1} \rangle$	m_1	q	$\frac{\langle J_1, m_1 1, 1q J_2, m_1 + q \rangle}{\sqrt{2J_2 + 1}}$	$ ME ^2$
4	4	$6\sqrt{5}$	-4	1	$-\frac{1}{3\sqrt{5}}$	4
4	3	6	-4	1	$\frac{1}{3}$	4

VI. LOW TEMPERATURE REQUIREMENTS

As we have mentioned the detection of very light axions, in the regime of a few μeV mass, crucially depends on the condition that the second level must be essentially free of electrons. To achieve this condition the target material should be brought at low temperatures. The critical temperature depends on the axion mass to be explored. The ratio of the probabilities of finding an accidental electron in the second level relative to the probability of finding one in the first level is given by the Boltzmann distribution probability:

$$P_{i,f} = e^{-m_a/kT} \quad (42)$$

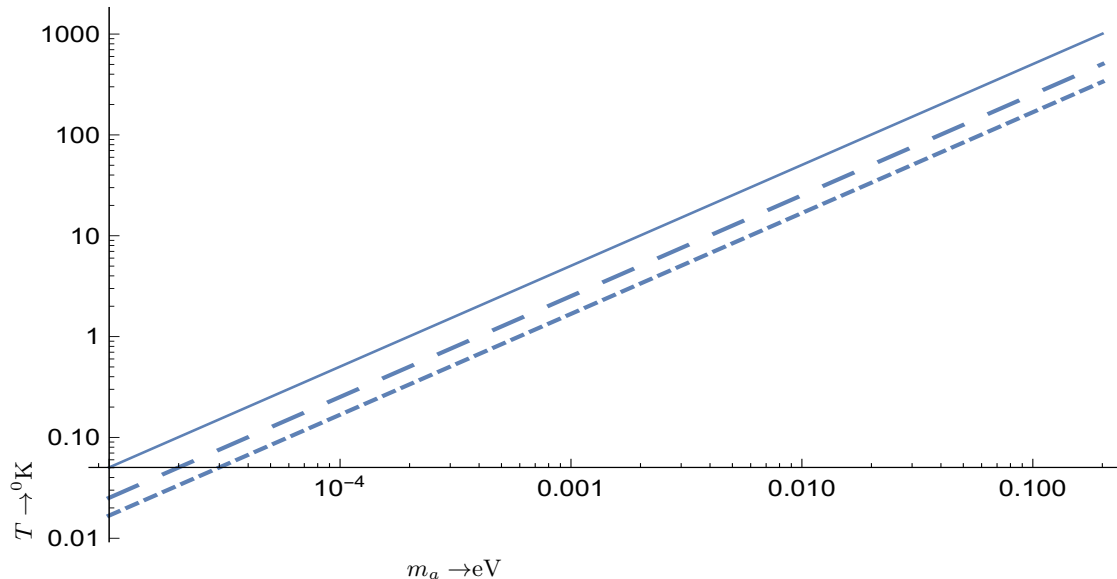


FIG. 6: The temperature in degrees Kelvin to be achieved is the region below the above curves, so that the population of the excited state by thermal electrons can be neglected. the continuous curve corresponds to relative probability of 10%, the long dash to 1% and the sort dash to 0.1%

Suppose that we demand this to be 10^{-x} . Then we find that

$$T \leq \frac{0.434m_a}{kx} \quad (43)$$

The condition on the temperature is given in Fig. 6. We thus see that, for axion mass $m_a = 0.4 \times 10^{-4}$ eV associated with a magnetic field $B=1T$, $T \leq 0.1$ K may be required. The situation may improve, of course, for larger magnetic fields. Anyway for axions heavier than 0.1 eV, very low temperatures are not required. Accidental backgrounds causing the excitation may be rejected from the resonance behavior, since it is unlikely that they are going to have a velocity distribution similar to that of the axions in the local frame.

There remains, however, an additional problem. For very light axions one has to develop detector materials, which at these low temperatures exhibit atomic structure. Ordinary atoms do not suffice. The ions of the crystal still exhibit atomic structure involving the bound electrons, as, e.g., the CUORE detector of Crystalline $^{130}\text{TeO}_2$ at low temperatures. The electronic states probably won't carry all the important quantum numbers as their corresponding neutral atoms, but they should possess the configurations connected by the spin excitations considered here. So one may prefer to consider targets which contain appropriate impurity atoms in a host crystal, e.g chromium in sapphire. As a matter of fact it is very encouraging that already there exist proposals involving rare-earth ions doped into solid-state crystalline materials [44] at low temperatures. In fact, if ion impurities are doped in crystals, one has to choose the target atoms in such a way that the corresponding ions can be isoelectronic to the atoms presented here and having the same configurations and terms. Since, as we shall see below, the expected rates for light axions are quite large, small impurities of 1 to 1000 or even 1/10000 may be adequate or one may relax the condition on the relative probability $P_{i,f}$.

It is, also, possible that one may be able to employ at low temperatures some exotic materials used in quantum technologies (for a review see [45]) like nitrogen-vacancy (NV), i.e. materials characterized by spin $S = 1$, which in a magnetic field allow transitions between $m = 0$, $m = 1$ and $m = -1$.

VII. SOME ESTIMATES ON THE EXPECTED RATES

We have seen that the event rate is given by Eq. (23). Its scale, computed with a cross section $\sigma_0 = 2.0 \times 10^{-47} \text{cm}^2$, extracted from the Borexino data, is shown in Fig. 3. We are now going to compute the total rates incorporating the

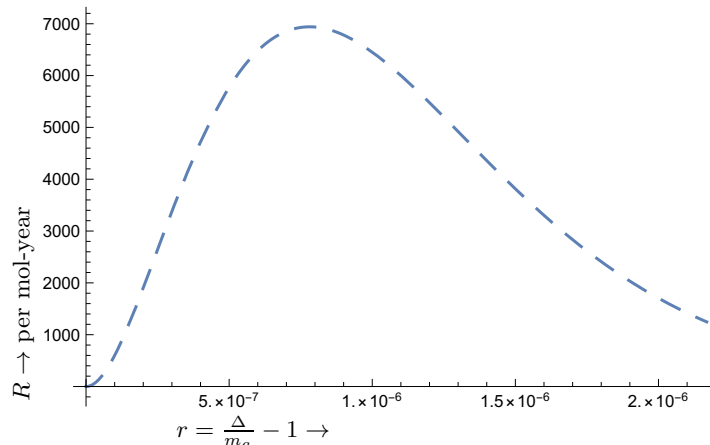


FIG. 7: The only possible transition is of A type. Now the transition energy is $\Delta = 6 \times 10^{-5} \frac{B}{1T} (1+r)$ eV. The extracted neutrino mass is given by the value of r_0 at the location of the maximum, $m_a = M_A(1-r_0)$, analogous to that of Eq. (44). The width is determined by $\Gamma = r_2 - r_1$, where r_2 and r_1 the locations at half maximum.

spin induced matrix elements $(C_{j_1, m_1, j_2, m_2, \ell})^2$ and the effects of the resonance. Our results will be presented in the form of suitable plots.

In the plots the resonance behavior will be apparent, but the location of the resonance as well as its width depend on the atom considered through the parameters m_i , $i = A, B, C, D$, which are functions of the spin orbit splitting ϵ as well as the energy δ due to the magnetic moment. These are given in section V. We should also indicate the event rate on the resonance for each type of transition A, B, C, D , which will not be the same for all of them due to the different axion mass and the spin induced matrix elements. For compactness of presentation we will put all this information for a given atomic target in the same plot. The event rate will be most economically presented for all transition types in the same figure as a function of $r = \frac{\Delta}{m_a} - 1$, with $\frac{\Delta}{m_a}$ covering the range of values allowed in the interval between $X = 0$ and $X = 2.84$, as discussed in section IV, in a fashion analogous to that of Fig. 5. The picture in this case will necessarily be more complicated, but we hope that, with the information provided, it will be understood, after the discussion of section IV.

Before we proceed further with the details of the rates of various atoms we should mention that the resonance condition given by Eq. (30) must be satisfied. It can now be written as

$$m_a = m_i (1 - \chi), \quad \begin{aligned} \chi &= 0.97 \times 10^{-6}, & i &= C \\ \chi &= 0.78 \times 10^{-6}, & i &= A, B, D \end{aligned} \quad (44)$$

A. One electron configurations

We will consider the following cases:

i) s-orbitals.

For such atoms the obtained rate is shown in Fig. 7.

ii) p-orbitals.

The event rate is exhibited in Fig. 8.

iii) d-orbitals.

The obtained event rates are shown in Figs 9-11.

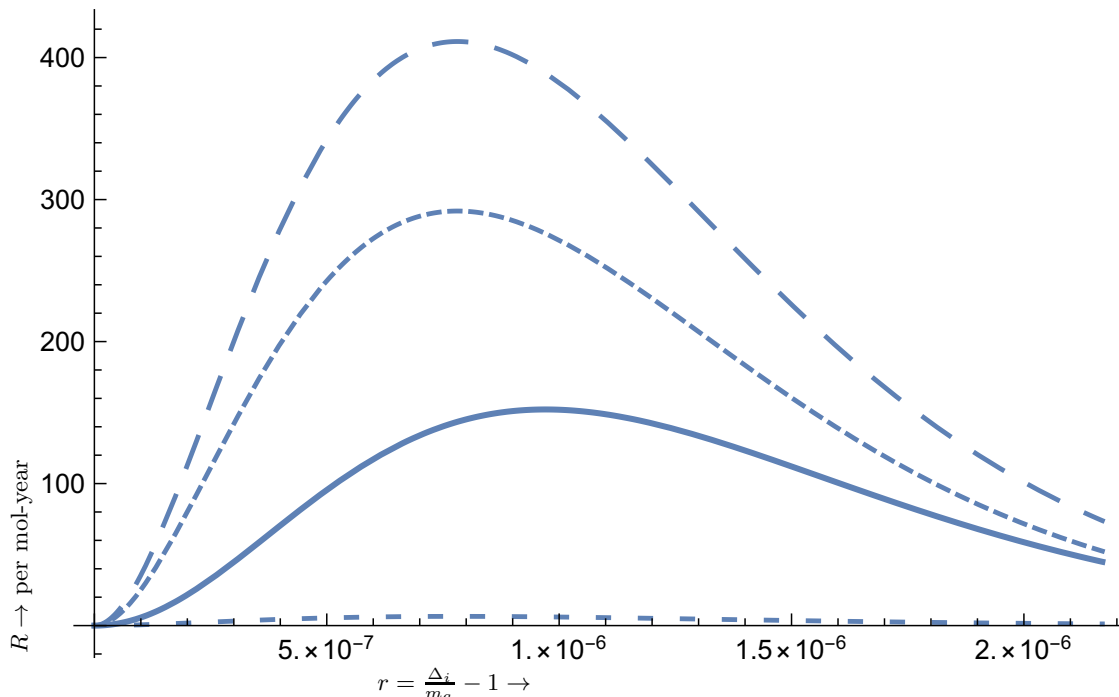


FIG. 8: The rate as a function of $r = \frac{\Delta_i}{m_a} - 1$, as a function of r , for transition types A, B, C, D indicated by long dash, short dash, solid line and intermediate dash respectively. Note that to make the type A fit in the picture we have suppressed it by the factor $C_g = 1/5$, i.e. its actual value is 5 times larger. In these plots the shape is essentially determined the velocity distribution. The extraction of the axion mass and the resonance width is determined as in Fig. 7, except that now $r_0 \rightarrow r_0^i$, $r_1 \rightarrow r_1^i$ and $r_2 \rightarrow r_2^i$, $i = A, B, C, D$. The obtained results for the axion mass and the extracted width may not agree exactly with those of Eq. (44) and (32) respectively due to the fact that the resonances here are not normalized. The parameters m_i are as follows: $m_A = \frac{2\delta}{3}$, $m_B = \epsilon - \frac{5\delta}{3}$, $m_C = \epsilon - \frac{\delta}{3}$, $m_D = \delta + \epsilon$. In the case of ^{13}Al considered here $\epsilon = 0.0130$ eV. For any other single particle p-orbitals only ϵ may be different.

B. Two electron configurations

In this case we will consider the two systems discussed in section V B 1, namely carbon and ^{22}Ti . In the first case the transition is $^3P_0 \rightarrow ^3P_1$, i.e. since the initial state is a $J = 0$, the A type transition is not available. The obtained rates are exhibited in Fig. 12. It may be useful to note that the Si atom has the same structure, except for the radial quantum, which is irrelevant here, and the fact that $\epsilon = 0.00956$ eV. Otherwise the situation is the same as in Fig. 12

The second target ^{22}Ti , the transition is $^3F_2 \rightarrow ^3F_3$, with the splitting of the spin orbit partners being relatively small. The obtained results are exhibited in Fig. 13. This use of such target, however, may suffer from the fact that ^{22}Ti normally exists in metallic form. It may be useful to note that the neutral Zr (Zr I) atom has the same structure, except for the radial quantum number, which is irrelevant here, and the fact that $\epsilon = 0.0707$ eV. Otherwise the situation is the same as in Fig. 13.

C. Many electron configurations

In this case we will consider the two targets described in section V B 2.

i) Transitions of the type $^3P_2 \rightarrow ^3P_1$.

The simplest such system is the oxygen with $n = 2$. As it has already mentioned, one may also consider sulfur (S I), which has the same configuration but different $n = 3$.

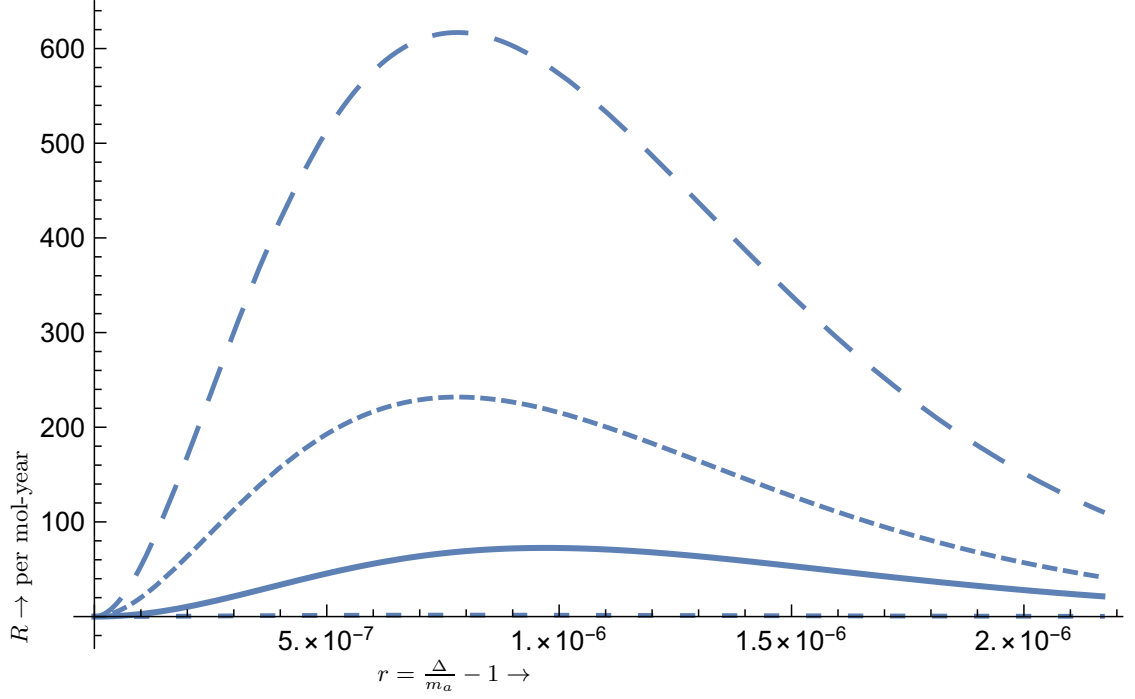


FIG. 9: The same as in Fig. 8 in the case of the atom $_{21}\text{Sc}$. The parameters m_i are as follows: $m_A = \frac{8\delta}{5}$, $m_B = \epsilon - \frac{9\delta}{5}$, $m_C = \epsilon - \frac{3\delta}{5}$, $m_D = \epsilon + \frac{3\delta}{5}$, with $\epsilon = 0.021\text{eV}$.

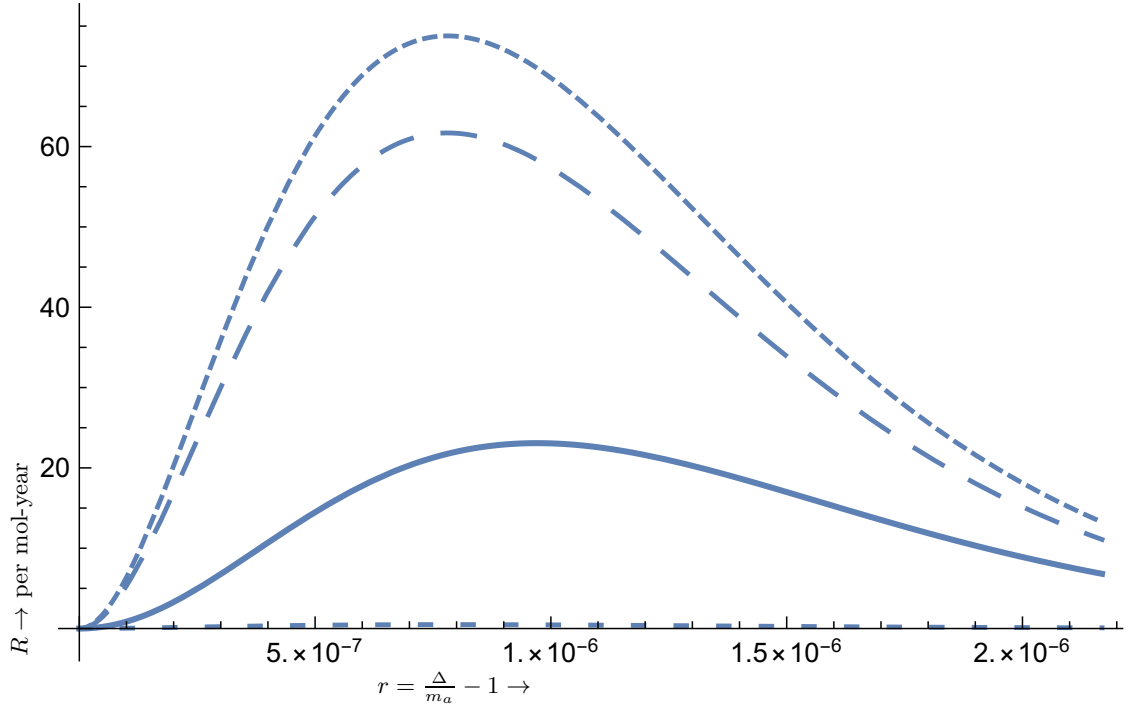


FIG. 10: The same as in Fig. 9 in the case of the atom $_{39}\text{Y}$, which also involves d-orbitals, but in this case $\epsilon = 0.066\text{eV}$. For transition type A the suppression factor $C_g = 1/10$ was employed, i.e the corresponding rate must be multiplied by 10.

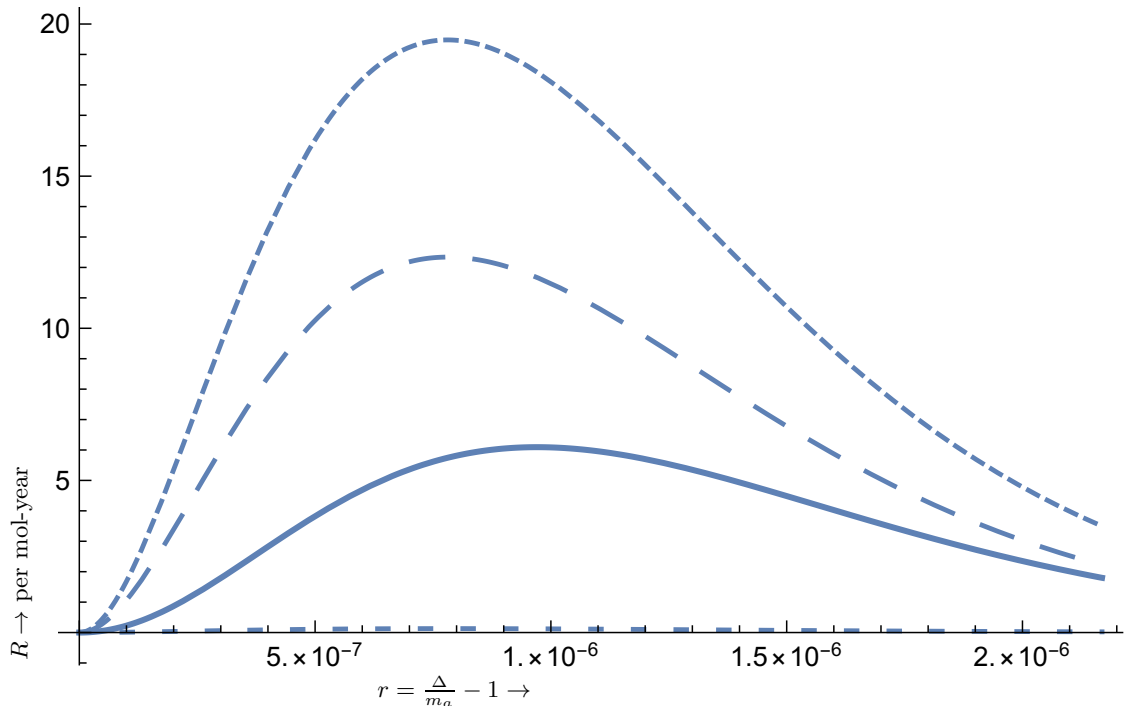


FIG. 11: The same as in Fig. 9 in the case of the atom ${}_{71}\text{Lu}$, which also involves d-orbitals, but in this case $\epsilon = 0.25\text{eV}$. Again for transition type A the suppression factor $C_g = 1/50$ was employed.

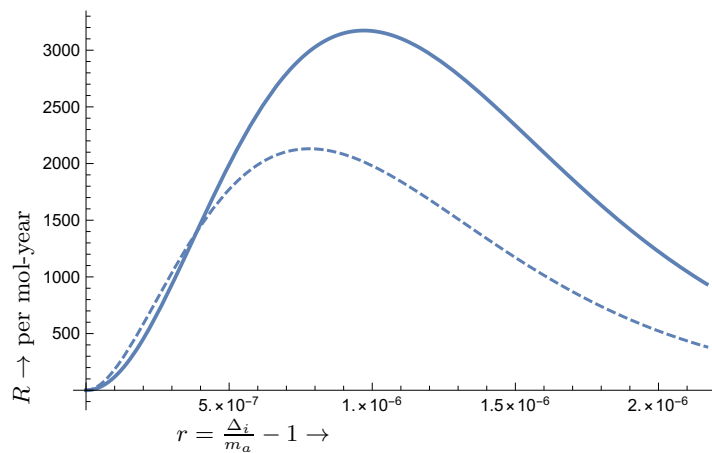


FIG. 12: The same as in Fig. 8 but for the C atom, with m_i as follows: $m_B = \epsilon - \frac{3}{2}\delta$, $m_C = \epsilon$, $m_D = \epsilon + \frac{3}{2}\delta$, $\epsilon = 0.002\text{ eV}$. The patterns B and D coincide, while the type A transition is not present.

ii) The second interesting example of many particle configurations is that of ${}_{26}\text{Fe}$ allowing the transition ${}^5D_4 \rightarrow {}^5D_3$. The obtained results presented in fig. 15.

At this point we should mention that, in the case of configurations with more than a single electron, some of the rates are enhanced due to the large spin interaction involved, see table II.

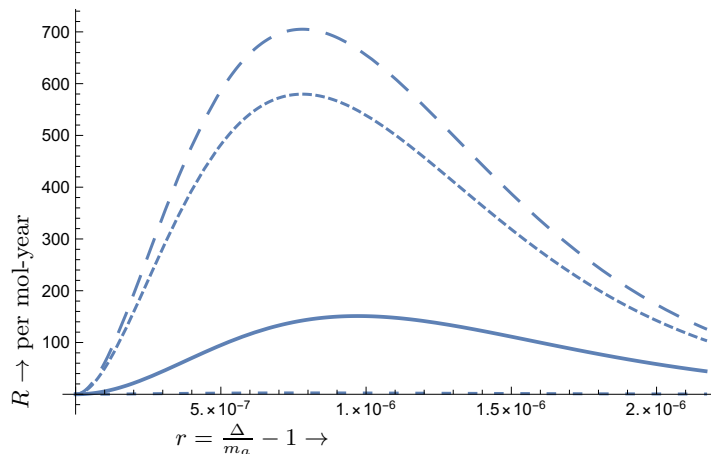


FIG. 13: The same as in Fig. 8 but for the Ti atom. For transition type A the suppression factor $C_g = 1/5$ was employed, i.e the corresponding rate must be multiplied by 5. Now m_i given by $m_A = \frac{28\delta}{9}$, $m_B = \frac{121\delta}{72} + \epsilon$, $m_C = \frac{115\delta}{36} + \epsilon$, $m_D = \frac{113\delta}{24} + \epsilon$, $\epsilon = 0.02$ eV. The type D transition is not visible.

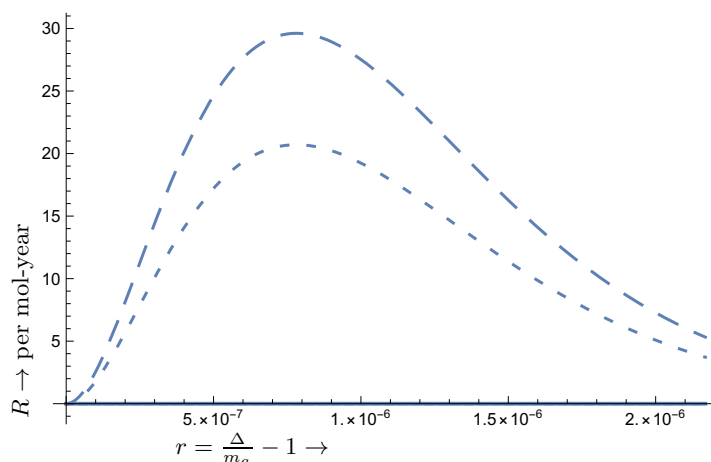


FIG. 14: The same as in Fig. 8 but for the oxygen target. The A term has been suppressed by a factor of 1/500, i.e. its actual value is 500 larger. Now m_i , $i = A, D$ with $m_A = \frac{5}{3}\delta$, $M_D = \epsilon + \frac{5}{3}\delta$, $\epsilon = 0.0197$ eV. The other two transition types B, C do not occur. The other two transition types B, C do not occur.

D. A summary of the obtained results

We have exhibited the results for the axion induced excitations for a number of atomic targets, see Figs 7 - 15. Similar results are expected for targets involving different radial functions with the same angular momentum structure as, e.g., in single particle structures involving s, p, and d orbitals, Si instead of C, Zr instead of Ti etc. The expected event rates, the width of the resonance and the dependence on the magnetic field will be the same. Only the extracted value of the axion mass from the B, C and D terms will be different, since it depends on the experimentally determined spin orbit splitting ϵ .

We have seen that in all atoms considered the expected resonances are very narrow and, since we have no experimental or theoretical information about the axion mass, they might be missed by experiments. The location of the resonance, however, depends on the magnetic field employed. One, thus, may consider a magnetic field whose magnitude is changing periodically from a minimum to a maximum value many times during the experiment. The oscillation period must be as short as possible and, in any case, very much shorter than the run time of the experiment. The latter must be longer than the time implied by the predicted event rate to compensate for the fact

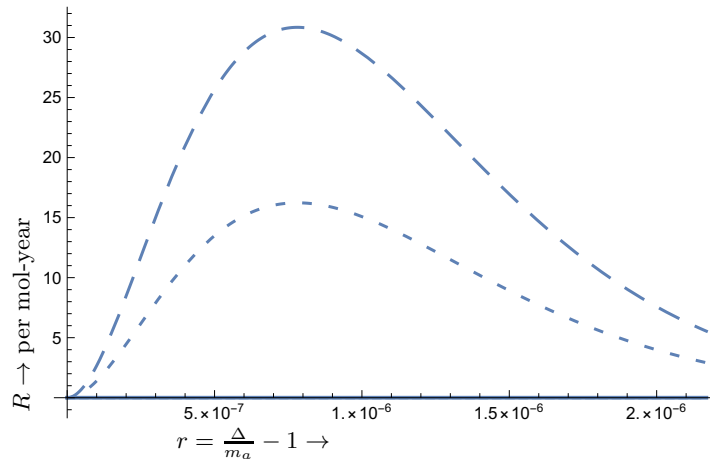


FIG. 15: The same as in Fig. 8 but for the iron target. The A term has been suppressed by a factor of $1/500$, i.e. its actual value is 500 larger. Now m_i , $i = A, D$ with $m_A = \frac{16}{5}\delta$, $M_D = \epsilon + \frac{16}{5}\delta$, $\epsilon = 0.05$ eV. The other two transition types B, C do not occur.

that only a fraction of the time the equipment is going to be at the right state of sensitivity for axion detection. With this arrangement one can perhaps see the axion provided its mass lies between $m_i|_{B=B_{min}}$ and $m_i|_{B=B_{max}}$ for $i = A, B, C, D$. This range depends on the atom considered. The most favored case is the one with as large as possible magnetic moment splitting. Thus in the case of the iron target one can detect light axion masses through the A term in the range of $\frac{16}{5}(\delta/n) \leq m_a \leq \frac{16}{5}\delta$. In particular for $n=100$ and $B = 1\text{T}$ one can detect axions in the mass range $2 \times 10^{-6}\text{eV} \leq m_a \leq 2 \times 10^{-4}\text{eV}$. This range is a bit wider than that of the dedicated experiments involving resonance cavities, such as the well known ADMX and ADMX-HF and CAP [22], searching for axion masses, see, e.g., [15], [17], [20], a summary [27] and a recent review [46] giving the range $10^{-6}\text{eV} \leq m_a \leq 10^{-4}\text{eV}$ (values $m_a \leq 4.4\mu\text{eV}$ have recently been excluded by ADMX [30]).

Similarly for heavier axions through the D term one gets a relation depending on the spin orbit splitting, in this case $0.05 + 2 \times 10^{-6}\text{eV} \leq m_a \leq 0.05 + 2 \times 10^{-4}\text{eV}$.

The width of the window, of course, can increase, if larger magnetic fields are employed, and the minimum can be selected as convenient.

Anyway such windows of axion mass can be open in atomic physics detection, provided that the sweep in frequency is smooth and gap-less, exploiting the feasibility of simultaneous scan of the frequency and the magnetic field in a prescribed way (see, e.g., [47], [48]).

This way one would think that the narrowness of the signal is beneficial rather than problematic, yielding an advantage of the atomic experiments.

VIII. CONCLUSIONS

In this paper we considered the possibility of direct detection of axion as a dark matter candidate by measuring the rates for axion induced atomic excitations. The essential input in our calculations was strength of the axion electron interaction g_{ae}/f_a and the axion flux on the detector. For the latter we have used the standard halo parameters with a Maxwell-Boltzman distribution transformed in the local frame. The strength of the interaction g_{ae}/f_a was assumed to be equal to the limit obtained from the Borexino experiment. This assumption allows axion masses in the range that can be exploited by spin induced atomic transitions. That is tens of μeV within members of the same multiplet, i.e. $|J_1, M_1 = -J_1\rangle \rightarrow |J_1, M_1 = -J + 1\rangle$, $J_1 \neq 0$ of the type A , and axion masses in the range $1\text{meV}-1\text{eV}$ involving transitions of to the type $|J_1, M = -J_1\rangle \rightarrow |J_2, M_2 = -J_1 + q\rangle$, $q = -1, 0, 1$, of the type B, C and D , allowed by the angular momentum selection rules.

Furthermore, since the axion is absorbed by the atom, the calculated cross section exhibits resonance behavior. The resulting pattern reflects the parameters of the velocity distribution in the local frame and the momentum dependence of the axion electron interaction. The obtained results depend, of course, on the atom considered, through the

parameters ϵ (the spin orbit splitting) as well as the δ (the energy splitting due to the magnetic moment interaction). The last two parameters determine the axion mass that can be detected, which is very close to the excitation energy. In addition the the resonance behavior can be exploited by experiments in minimizing any background events.

In the special case of the type *A* transitions the obtained rates, as shown at the top of the resonance, are quite large as a result of the large axion flux. The highest rates obtained occur in the case of light axions. They involve all the $s_{1/2}$ transitions in any atom and the *A* type transitions and for the many electron configuration atoms like Oxygen and ^{28}Fe , namely $R = 7.0 \times 10^3$, $R = 1.4 \times 10^4$ and $R = 1.4 \times 10^4$ per mole-y respectively. The experimental detection difficulty in this case is not connected with the expected rate but, as explained in section VI, with the very low temperature behavior of the target. The excited state must be essentially empty of electrons. Furthermore the target must exhibit atomic behavior at such low temperatures. It may be an advantage that such high rates allow one to consider the atom of interest in the form of an impurity, at the level $1/10^3$ or even $1/10^4$ in an otherwise inert target.

For the *B*, *C*, and *D* type transitions the low temperature requirements are not very stringent. The expected rates, as appearing at the tops of some of the the *B*, *C*, *D* patterns in the figures, are much smaller than those of the *A* terms, see Figs 8-15, but perhaps detectable. In the case of the ^{22}Ti a rate as high as $R = 5.0 \times 10^2$ per mole-y is obtained.

The main experimental problem for all types of transitions is due to the fact that all resonances are very narrow and they might be missed by the experiments. This is, unfortunately, so since there is no experimental or theoretical guide about the expected value of the axion mass. We have seen, however, that, if a suitable periodic magnetic field is selected, whose magnitude is in a appropriate range and its period is very much smaller than the experimental run time, a window of axion mass, in the range of a fraction of an meV wide, becomes open, which may be adequate.

Acknowledgments

J.D.V is happy to acknowledge that this work was supported by IBS-R017-D1-2020-a00. Special thanks to professor Yannis Semertzidis, director of the Center for Axion and Precision Physics Research, IBS, at KAIST University, for his hospitality, encouragement and useful discussions. All authors are indebted to Professor P. Sikivie for a careful reading of the manuscript and his very useful comments and suggestions as well as bringing to their attention the need of simultaneous scan of frequency and magnetic field. Special thanks to Professor H. Ejiri for clarifying some aspects of the experiment proposed in this work.

-
- [1] R. Peccei and H. Quinn, Phys. Rev. Lett **38**, 1440 (1977).
 - [2] S. Weinberg, Phys. Rev. Lett. **40**, 223 (1978).
 - [3] F. Wilczek, Phys. Rev. Lett. **40**, 279 (1978).
 - [4] J. E. Kim, Phys. Rev. Lett. **43**, 137 (1979).
 - [5] M. A. Shifman, A. Vainshtein, and V. I. Zakharov, Nuc. Phys. B **166**, 493 (1980).
 - [6] M. Dine, W. Fischler, and M. Srednicki, Phys. Lett. **B 104**, 199 (1981).
 - [7] A. Zhitnisky, Sov. J. Nuc. Phys. **31**, 260 (1980), in Russian.
 - [8] L. F. Abbott and P. Sikivie, Phys. Lett. **B120**, 133 (1983).
 - [9] M. Dine and W. Fischler, Phys. Lett. **B120**, 137 (1983).
 - [10] J. Preskill, M. B. Wise, and F. Wilczek, Phys. Lett. **B120**, 127 (1983).
 - [11] S. J. Asztalos et al., Phys. Rev. Lett. **104**, 041301 (2010), the ADMX Collaboration, arXiv:0910.5914 (astro-ph.CO).
 - [12] L. Duffy et al., Phys. Rev. Lett. **95**, 09134 (2005), for the ADMX Collaboration.
 - [13] A. Wagner et al., Phys. Rev. Lett. **105**, 171801 (2010), for the ADMX collaboration; arXiv:1007.3766 (astro-ph.CO).
 - [14] I. G. Irastorza and J. A. García, JCAP **1210**, 022 (2012), arXiv:1007.3766 (astro-ph.IM).
 - [15] T. M. Shokair, J. Root, K. Bibber, et al., international Journal of Modern Physics A, arXiv:1405.3685 [physics.ins-det].
 - [16] P. Sikivie, Phys. Rev. Lett. **51**, 1415 (1983).
 - [17] J. Primack, D. Seckel, and B. Sadoulet, Ann. Rev. Nuc. Par. Sc. **38**, 751 (1988).
 - [18] S. Aune et al., Phys. Rev. Lett. **107**, 261302 (2011), arXiv:1106.3919; CAST Collaboration.
 - [19] A. Arvanitaki, S. Dimopoulos, S. Dubovsky, N. Kaloper, and J. March-Russell, Phys. Rev. D **81**, 123530 (2010), arXiv:0905.4720.
 - [20] I. P. Stern, ArXiv 1403.5332 (2014) physics.ins-det, on behalf of ADMX and ADMX-HF collaborations, Axion Dark Matter Searches.

- [21] G. Rybka, The Axion Dark Matter Experiment, IBS MultiDark Joint Focus Program WIMPs and Axions, Daejeon, S. Korea October 2014.
- [22] Center for Axion and Precision Physics research (CAPP), Daejeon 305-701, Republic of Korea. More information is available at http://capp.ibs.re.kr/html/capp_en/.
- [23] S. J. Asztalos et al., Nucl. Instr. Meth. in Phys. Res. **A656**, 39 (2011), arXiv:1105.4203 (physics.ins-det).
- [24] S. Lee, S. Ahn, J. C. B. R. Ko, and Y. K. Semertzidis, Phys. Rev. Lett. **124**, 101802 (2020).
- [25] D. Kim, J. Jeong, S. W. Youn, Y. Kim, and Y. K. Semertzidis, JCAP **03**, 066 (2020).
- [26] Y. K. Semertzidis et al. (2019), axion Dark Matter Research with IBS/CAPP, arXiv:1910.11591 [physics.ins-det].
- [27] G. Raffelt, Astrophysical Axion Bounds , IBS MultiDark Joint Focus Program WIMPs and Axions, Daejeon, S. Korea October 2014.
- [28] N. Du et al., Phys. Rev. Lett. **120**, 151301 (2018).
- [29] T. Braine et al., Phys. Rev. Lett. **124**, 101303 (2020).
- [30] C. Bartram et al., Phys. Rev. Lett. **127**, 161903 (2021).
- [31] K. Zioutas and Y. Semertzidis, Phys. Lett. A. **130**, 94 (1988).
- [32] H. B. T. Tan, V. V. Flambaum, I. B. Samsonov, Y. V. Stadnik, and D. Budker, interference assisted resonant detection of axions, arXiv:1803.09388 (hep-ph), (astro-ph.CO), (physics.atom-ph).
- [33] V. V. Flambaum, I. B. Samsonov, H. B. T. Tan, and D. Budker, coherent axion-photon transformations in the forward scattering on atoms, arXiv:1803.01783 (hep-ph), (physics.atom-ph).
- [34] P. Sikivie, Phys. Rev. Lett. **113**, 201301 (2014).
- [35] G. Bellini et al. (The Borexino Collaboration), Phys. Rev. D **85**, 092003 (2012), arXiv:1203.6258 [hep-ex].
- [36] J. D. Vergados, J. Phys. G **47**, 095007 (2020), arXiv:1605.05413 (hep-ph).
- [37] M. Gorghetto and G. Villadoro, ArXiv **1812.01008**, 1 (2018), arXiv:1812.01008 [hep-ph].
- [38] J. Vergados, P. C. Divari, and H. Ejiri, AHEP **2028**, 7373365 (2022), <https://doi.org/10.1155/2022/7373365>.
- [39] G. G. di Cortona, E. Hardy, J. P. Vega, and G. Villadoro, JHEP **01**, 034 (2016), arXiv:1511.02867, (hep-ph), (hep-ex), (hep-lat).
- [40] A. Ringwald and K. Saikawa, Phys. Rev. D **93**, 085031 (2016), arXiv:1512.06436 [hep-ph].
- [41] M. Srednicki, Nucl. Phys. B **260**, 689 (1985).
- [42] J. D. Vergados and Y. Semertzidis, Nuc. Phys. B **897**, 821 (2016), arXiv:1601.04765 (hep-ph).
- [43] J. Vergados, *Group and Representation Theory* (World Scientific, 1st edition, 2017).
- [44] C. Braggio, G. Carugno, F. Chiossi, A. D. Lieto, M. Guarise, P. Maddaloni, A. Ortolan, G. Ruoso, L. Santamaria, J. Tasseva, et al., Scient. Rep. **7**, 15168 (2017).
- [45] M. W. Doherty, N. B. Manson, P. Delaney, F. Jelezko, J. Wrachtrup, and L. C. L. Hollenberg, Phys. Rep. **528**, 1 (2013), arXiv:1302.3288.
- [46] A. Ringwald (2016), proc. of the Neutr. Osc. Workshop 2016, 4 - 11 September, 2016, Otranto, Lecce, Italy; arXiv:1612.08933 [hep-ph].
- [47] D. Delande, K. T. Taylor, M. H. Halley, T. van der Veldt, W. Vassens, and W. Hogervorst, J. Phys. B: At. Mol. Opt. Phys. **27**, 2771 (1994).
- [48] R. K. Leach, *Fundamental principles of engineering nanometrology* (Oxford: Elsevier Science, 2010).

IX. APPENDIX: THE MODULATION OF THE WIDTHS

The modulation of the widths can be simply included by making in the local frame we make the replacement:

$$F_0(X) \rightarrow e^{-\delta \cos \alpha - \delta^2} F_0 \left(X \left(\frac{1}{2} \delta \cos \alpha + 1 \right) \right), \quad (45)$$

where α is the phase of the Earth, $\alpha = 0$ around June 3rd, and δ the ratio of Earth's velocity around the sun divided by the sun's velocity around the galaxy, $\delta \approx 0.135$. We thus get a time variation of the width shown in Fig. 16. We see that the effect is small, the difference between the maximum and the minimum is less than 3%, almost the same with that obtained in the axion to photon conversion [42]. We note, however that, in addition to the seasonal dependence we have a dependence on the magnetic quantum numbers of the states involved. The variation in the case of $m_1 \neq m_2$ is almost twice as large compared to that with $m_1 = m_2$.

It is amusing to know that the dispersion $\sigma = \sqrt{\langle X^2 \rangle - \langle X \rangle^2}$ also exhibits a time dependence (see Fig. 17).

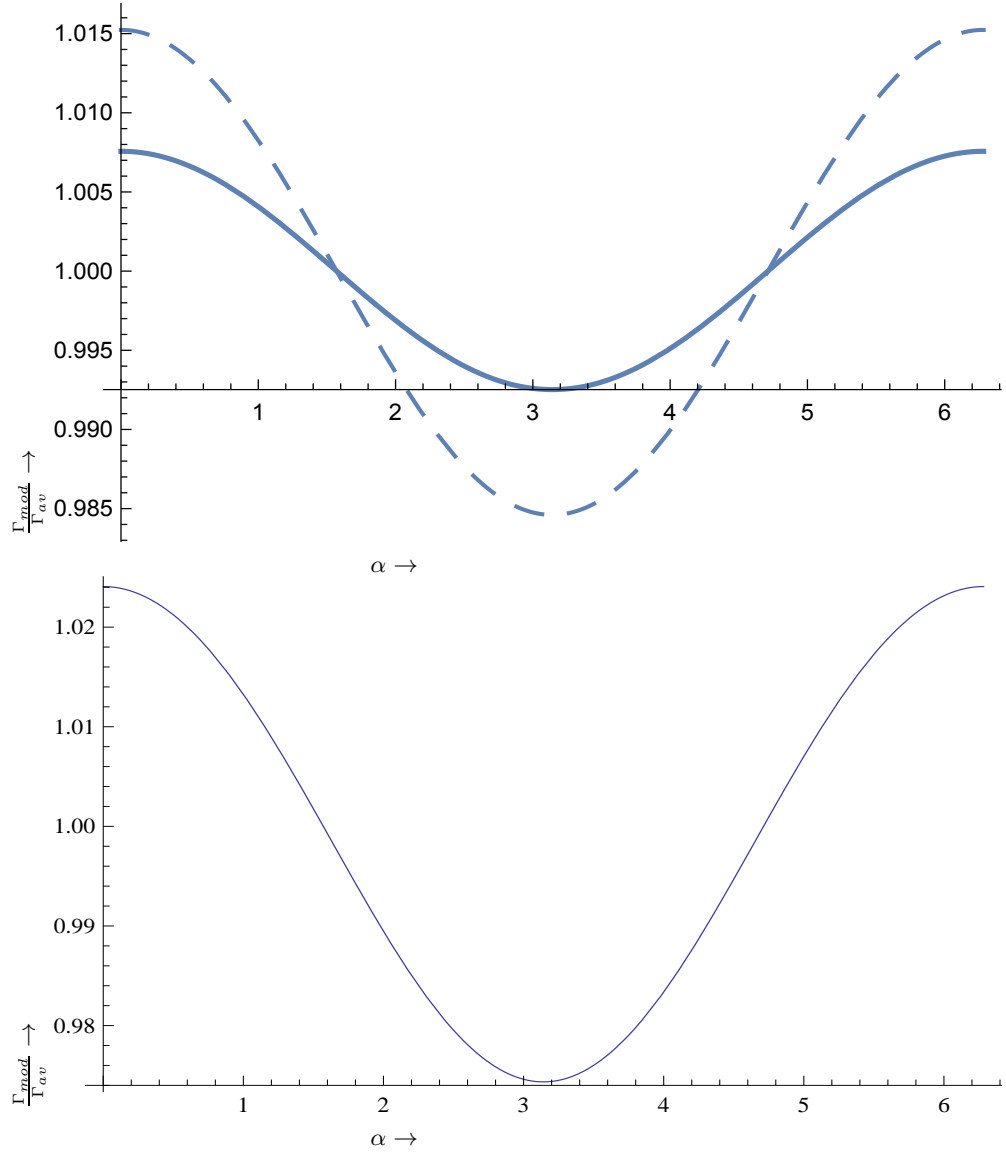


FIG. 16: In the top panel we exhibit the modulation of the width Γ , relative to its average value, as a function of the phase of the Earth. The notation for the curves is the same as in Fig. 4. For comparison we present in the bottom panel the modulation curve obtained in the case of the standard axion to photon conversion, obtained with the same halo parameters [42].

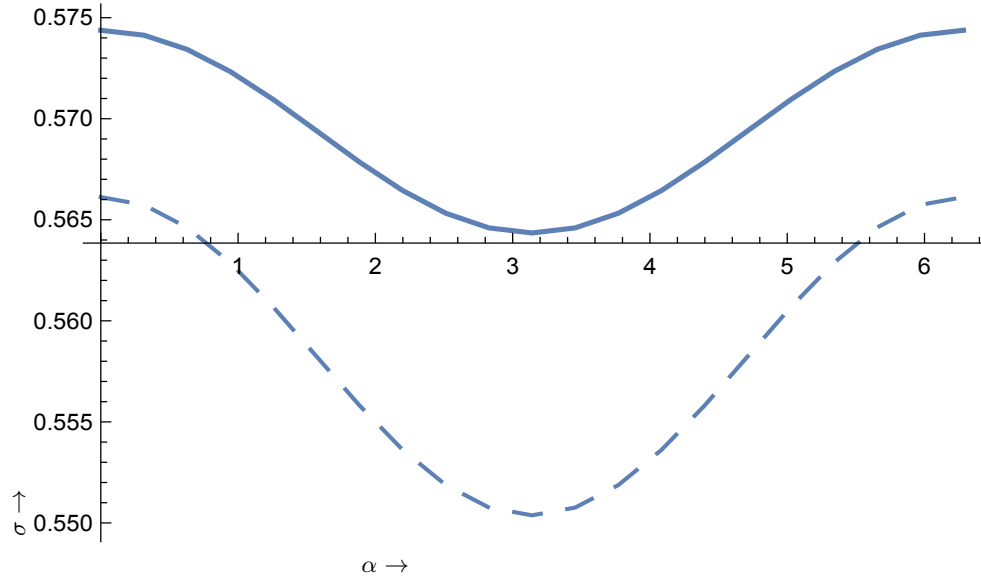


FIG. 17: The time variation of the width for axion absorption by an atom due to the motion of the Earth. The notation for the curves is the same as in Fig. 16.